UNIVERSITY OF CALIFORNIA SAN DIEGO

Utilizing cloud speed data to predict the time of occurrence of irradiance drops

A Thesis submitted in partial satisfaction of the requirements for the degree Master of Science

in

Engineering Sciences (Mechanical Engineering)

by

Venkat Suman Roy

Committee in charge:

Professor Jan Kleissl, Chair
Professor Renkun Chen
Professor Carlos Coimbra

2019

The Thesis of Venkat Suman Roy is approved and acceptable in quality and form for publication on microfilm and electronically:

_____

_____

_____

Chair

University of California San Diego

2019

TABLE OF CONTENTS

LIST OF FIGURES

LIST OF TABLES

ABSTRACT OF THE THESIS

Utilizing cloud speed data to predict the time of occurrence of irradiance drops

by

Venkat Suman Roy

Master of Science in Engineering Sciences (Mechanical Engineering)

University of California San Diego 2019

Professor Jan Kleissl, Chair

The ability to predict short-term fluctuations in irradiance is a necessary component of ensuring the reliability of a solar PV system at a given location. Local cloud phenomena that are responsible for these changes are dynamic and difficult to model; on-site measurements of irradiance provide an easy way to capture these effects. In this study, cloud movement is tracked in time through its effect on irradiance signals at different locations and compared with the estimates of the travel time from cloud speed data. The results showed a good correlation between the two different time lags for a short separation distance of 228m, but there was almost no relation for higher distances. Using different similarity measures like Correlation, Euclidean distance or the location of Local Minima for the signal analysis didn't affect the results widely for the shortest separation distance.

1. INTRODUCTION

Solar photovoltaic power continues to play an important role in shifting the energy mix towards cleaner sources, and like other renewables, solar energy is intermittent and non-dispatchable. Unlike conventional energy sources, it introduces higher variability and uncertainty into the energy supply, requiring additional balancing mechanisms, energy storage options and backup resources to adequately meet the demand. Although manufacturing costs of solar PV panels are dropping, above factors can increase the cost of power plant operation, distribution through electric utilities, and eventually the price of electricity for the consumer[1]. A prior knowledge of the resource variability through different forecasting methods can help mitigate these effects and facilitate higher penetration of solar power in the electricity market [2].

The resource characterization for solar power generation involves estimating the Global Horizontal Irradiance (GHI), the main input for a solar PV system, at the given location over multiple time horizons. The changes in irradiance are governed by the sun's position relative to this location and the atmospheric conditions. Over long time horizons ranging from a few hours to day-ahead to even seasonal oscillations, the changes can be forecasted using numerical weather prediction models and satellite imaging[3]. In addition to these variations that influence irradiance over large areas like entire cities, local cloud movement can cause rapid fluctuations in irradiance in a window of few seconds to minutes, depending on the cloud's motion and it's physical properties. Given their localized and fleeting nature, it's difficult to model clouds using physics-based methods in time to forecast their effects. Ground-based sky imagers have been used to track cloud motion[4], images of the cloud are processed using machine-learning techniques to derive cloud speeds and translate them to changes in the irradiance distribution. This can be

computationally intensive, alternatively, irradiance monitoring sensors can be used to capture the spatio-temporal variations caused by clouds.

Irradiance data at one location can be analyzed using Statistical methods [5] like auto-regression, moving average, to predict short-term fluctuations (few minutes) with some improvement over persistence models. Given the complexity of variation in the data, machine learning techniques have also been applied for short-term irradiance forecasts [5]. In addition to historical GHI data required to train these models, they can incorporate exogenous inputs like cloud motion vectors (CMV's) to improve performance. Another approach to explicitly use cloud speeds is through cloud advection-based methods [6,7] where the cloud motion vectors are used to project irradiance measurements across sensors based on separation distance and relative orientation. The spatial & temporal resolution of the sensors i.e. distances separating the sensors and frequency of irradiance recorded can influence the forecasting performance and window, for example the correlation between irradiance signals decreases with higher separation distance [8].

In this study, the effectiveness of CMV in forecasting the occurrence of relative variation between irradiance signals at nearby locations is examined using three pairs of sensors with different separation distances. The spatial variation of irradiance in real-time is translated to time lags between the locations by time-shifting signals to maximize their similarities. Correlation, Euclidean distance and a Minima Matching algorithm were used to measure these similarities, and the resulting time-lags were compared with the time taken by the clouds to travel between the locations. CMV's used for that calculation were obtained using a cloud speed sensor described in Wang et al [9].

2. METHODOLOGY

2.1 Signal Analysis Method

If a cloud passing over an irradiance sensor caused a simple rectangular drop in the signal it would be easy to track across multiple sensors with great precision, but irradiance drops can have complex shapes usually accompanied by a lot of sub-minute fluctuations that can be random, leading to a noisy signal. Several cloud properties could contribute to the above effect, even within a single cloud the thickness and composition could be non-uniform, which affects how the light passing through is dispersed and subsequently the incident irradiance. Figure 1 shows an irradiance signal from one of the sensors, it has a few major drops (over 50%) in power but there are also a lot of much smaller dips that are random and make it difficult to compare similarities in drops across different sensors.

Smoothing out the signal using a moving average removes the high-frequency noise but would also remove some of the high-magnitude drops that occur in very short time periods. One approach to avoid this is to locate the points where the slope of the signal changes the most and use those points to reconstruct the signal by linear interpolation between those points. Based on the required no. of changepoints the signal can be divided into windows of fixed time intervals. Within each window, any given point divides the remaining signal into two sets which are then fitted onto two straight lines. The total sum of residual error from the linear regression in both segments is minimized to locate a changepoint in each window. The function *findchangepts* () in MATLAB was used for this purpose with the statistical measure input set to ‘linear’.

An example of a modified signal is show in Figure 1 (Red), the low-magnitude fluctuations have been excluded without losing the relevant drops. The level of filtered noise is controlled by

the no. of points selected for a given window, in Figure 1 a 10-minute window was modeled using 10 points; an average of 1 change-point per minute.

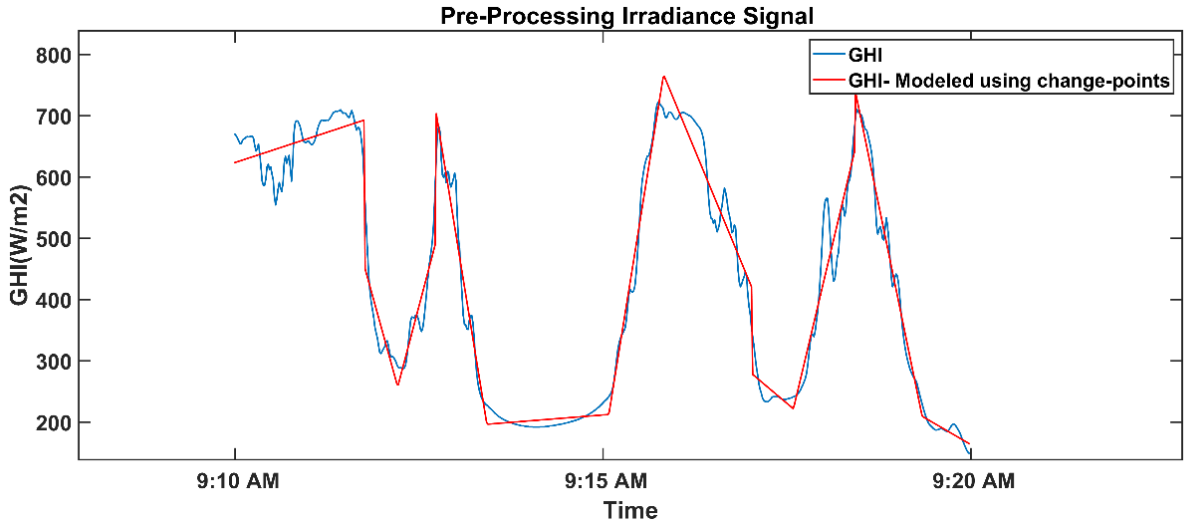

Figure 1: Pre-processing Irradiance Signal by linear interpolation using changepoints (A Sample of 10 min window of signal recorded at EBU2)

Irradiance signals at different locations can be compared to derive a time lag that should ideally match with those derived from cloud motion vectors. There will be deviations from this assumption since clouds are dynamic and their properties will change in transit. This leads to varied effects on the irradiance signal at different locations, as the separation distance grows the deviations become more prominent. Even for short distances (under 1 km) considered in this study, different methods of studying the signal similarities could affect the outcome. In order to find a time lag that accurately represents the movement of the cloud, the similarities between the signals are compared using the three different methods described below.

i. Cross-Correlation

This is the most common method used in time-series analysis to find time lag, the signal values are locally detrended and multiplied to find correlation at different time shifts. The maximum correlation indicates the closest similarity and the corresponding time shift gives the time lag. A pair of irradiance signals are shown in the first plot of Figure 2, within a 10 min window there is big drop from around 600 W/m2 to 200 W/m2 in both signals but at different times. Initially the correlation coefficient is -0.08, by shifting the second signal (red) to increase this coefficient, a maximum of 0.47 can be achieved, as shown in the second plot. The time lag at this point is 156 seconds, and the major drop is more aligned than before. This point is also shown on a plot of the normalization coefficient with time shift, the sign depends on the which of the signal is defined as the reference.

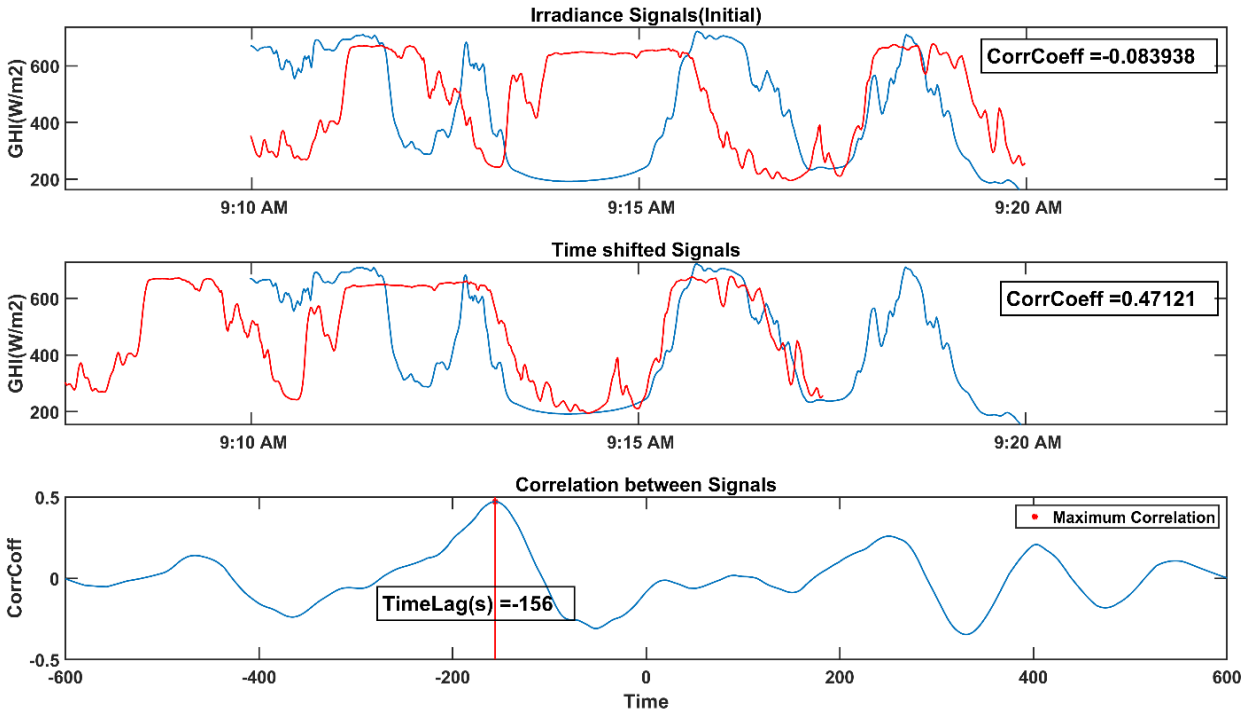

Figure 2: Cross- Correlating Signals: Initial signals recorded (Top), Time shifted signal to maximize correlation (Middle) and Variation of correlation coefficient with time lag (Bottom).

Apart from the big drop, there are some portions of the signal that might be less aligned after time-shifting the signal, which negatively affects the correlation coefficient. This occurs since the duration of the cloud event can be shorter than the time window analyzed, the misalignment in the remaining portion will have lower impact when the cloud-related irradiance variation is of higher magnitude.

ii. Euclidean Distance

Euclidean distance between the irradiance signals is same as the Root Mean Squared Error if one of the signals is being using to predict the values of the other. Figure 3 shows the signals for the same time window considered in the previous method. Since RMSE represents the dissimilarity between signals, its minimum point gives the time lag at which the signals are most similar. In this example it occurs at a lag of 151 seconds, as shown in the RMSE vs time lag plot. The corresponding shifted signals are more aligned in terms of the major drop just like the previous method, but there is a slight difference in the time lag. Since the entire window is used for the calculation, the smaller variations that might not be cloud related also affect the RMSE, leading to a high RMSE value even after the shifting the signal.

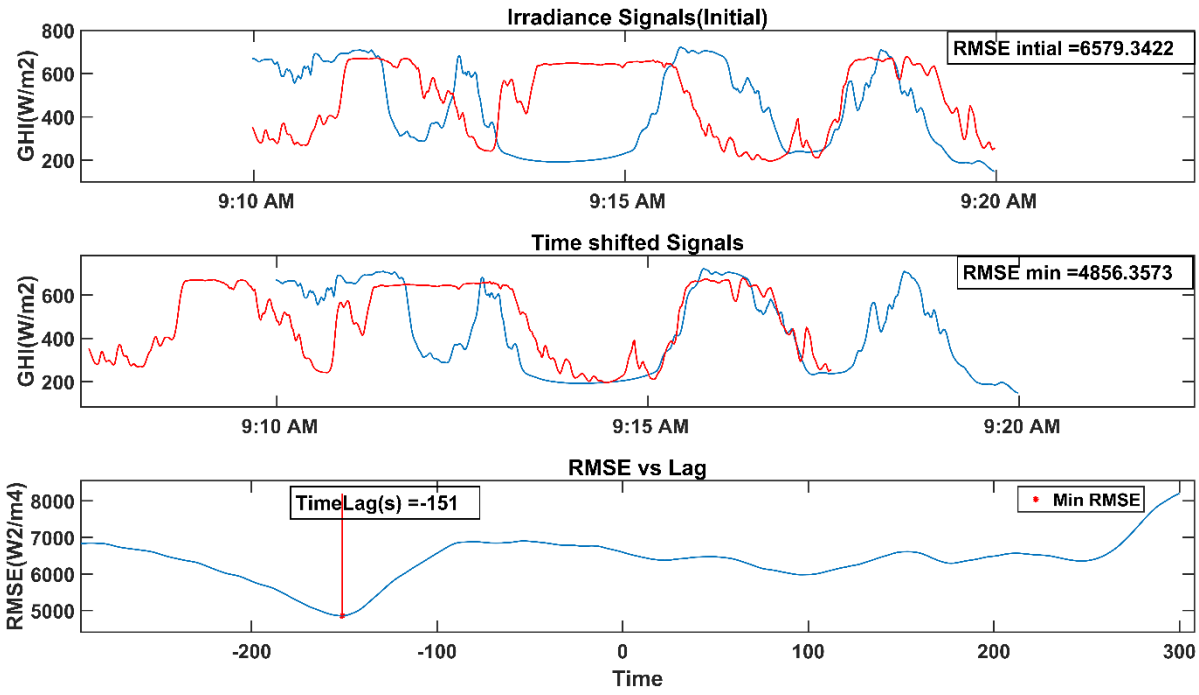

Figure 3: Minimizing Euclidean Distance between Signals: Initial recorded irradiance signals (Top), Time shifted signal to minimize Euclidean distance (Middle) and Variation of Euclidean distance/RMSE with time lag (Bottom).

iii. Minima Matching

The previous methods use all points in the signal to compare similarities, in this method only the minimum point in a window is used to find time lags. Similar to previously used peak matching algorithms[10], the time lag is obtained by calculating the time difference between the minimum points of the signals. Figure 4 shows irradiance signals considered along with their minima which were separated by 172 seconds. Although most of the details of a signal drop are ignored, isolating the effect of the cloud to the minimum point avoids involving a lot of complex variations within the signal in the analysis, which can be time consuming and computationally intensive.

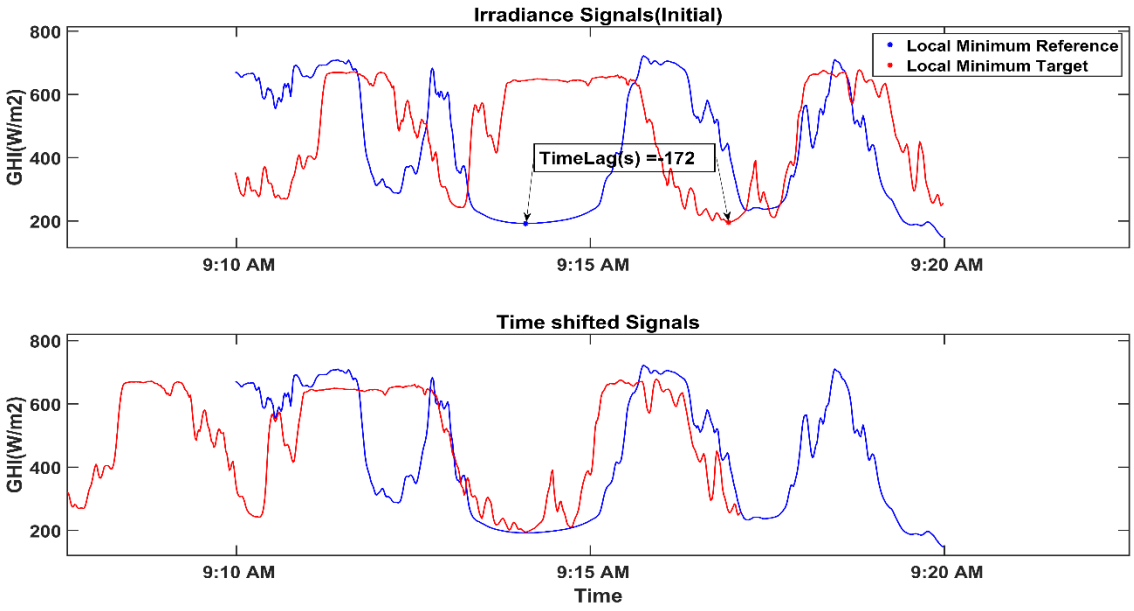

Figure 4: Minima Matching: Initial recorded irradiance signals (Top), Time shifted signal to match minima (Bottom)

The above three methods discuss ways to compare irradiance signals, but they were only applied to a single window. To compare irradiance signals for an entire day, the signal needs to be split into windows using a search method. Segmenting the signal into windows uniformly over the entire day is the simplest approach and can be applied to all the above methods. An additional approach that was used is placing the windows around the local minima of the signal since the most of the cloud-related irradiance drops can be isolated to where the drop-in signal is the most. This approach can help with centering the desired variation within the search window of the reference signal, which in turn increases the chances of finding the same variation in the target signal within the same time window. Section 2.4 demonstrates the above signal analysis methods on the available input data.

2.2 Input Data

The irradiance data was collected at the 4 locations shown in Figure 5, EBU2 location was used as the reference while other three locations, CMRR, TIOG and BMSB were considered the targets for forecasting. Data was available for three days for the BMSB and EBU2 locations, 8th 10th & 11th Oct 2017 and the CMRR & TIOG data was limited to one day, 10th Oct and 8th Oct respectively. Data availability is summarized in Table 1. GHI data was recorded at using pyranometers with a 1s sampling rate. Separation distance between reference (EBU2) and the target varies as follows, 228m-CMRR, 1004m-TIOG and 681-BMSB. Cloud motion vectors were recorded using a cloud speed sensor located at EBU2. The sampling rate is variable since CMV's were observed only when there was a cloud event. CMV Data availability was limited to three days, 8th, 10th and 11th Oct.

Figure 5: Map of the locations where data was collected, EBU2 was the reference location for irradiance signals and the cloud speed sensor was also located at that location

Table 1: Data Available at Different Locations

Location	Parameter Recorded	Sampling Rate	Dates of Availability	Distance from Ref.(m)
EBU2(Ref)	GHI	1s	8,10,11th Oct 2017	-
	CMV	~12s	8,10,11th Oct 2017	-
CMRR	GHI	1s	11th Oct 2017	228
BMSB	GHI	1s	8,10,11th Oct 2017	681
TIOG	GHI	1s	8th Oct 2017	1004

For each pair of locations there are four input variables required, the GHI from reference and target locations, cloud speed and direction from reference location. Figure 6 shows the plot of these variables for the CMRR & EBU2 locations on 11th Oct. Irradiance (GHI) data has a lot of sub-minute fluctuations indicating cloudy conditions. This is also implied from the availability of cloud speed data during that day, which would not be possible on a clear day. Cloud direction shifts from 0 to 360 sometimes, which is expected from a circular setup used in the cloud speed sensor. In the following sub-sections, the analysis is demonstrated using this pair since it has the shortest separation distance. The results for the remaining pairs on different days are discussed in the next section.

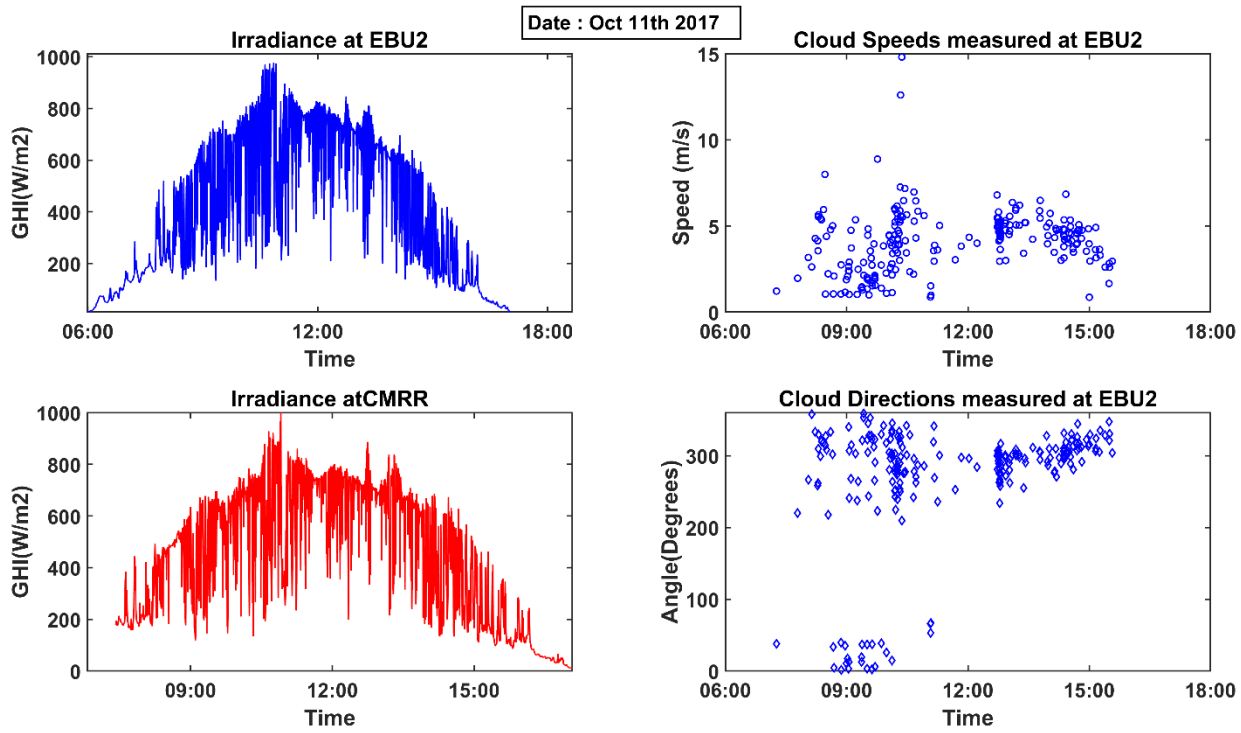

Figure 6 : Input Data for CMRR & EBU2 Pair on 11th Oct – EBU2 Irradiance (Top Left) , Cloud Speed (Top Right), Cloud Directions (Bottom Right), CMRR Irradiacne (Bottom Left)

2.3 Time Delay from Cloud Motion Vectors

Using the cloud speed and direction measured at the reference location, the time taken for the cloud to reach the target can be estimated. The cloud shadow can cover large areas, so even if the cloud is not heading directly towards the target location, a portion of the cloud might still affect the irradiance signal. In order to calculate time delays from all the cloud speeds recorded, they are projected along the direction of the line connecting the reference and target locations. Projection angle is found using the cloud direction and the co-ordinates of the locations.

Although most clouds would affect both locations given the distance is short enough, there are some cases that should be filtered. In the case when a cloud is traveling in almost a

perpendicular direction to the target , i.e. projection angle is close to 90/270 degrees, the cloud may not affect the irradiance at the target, or if the cloud speed is too low the effect of the cloud may not show up on the irradiance signal within a short time window of analysis. Since projection speed depends on both cloud speed & direction, in both these cases its value is will be reduced, so a minimum cut-off is required to filter out values below a certain point. For this study, the projection speed was cut-off at a minimum of 0.5 m/s, but a lower or higher value can be selected based on the desired range of time lags from the analysis.

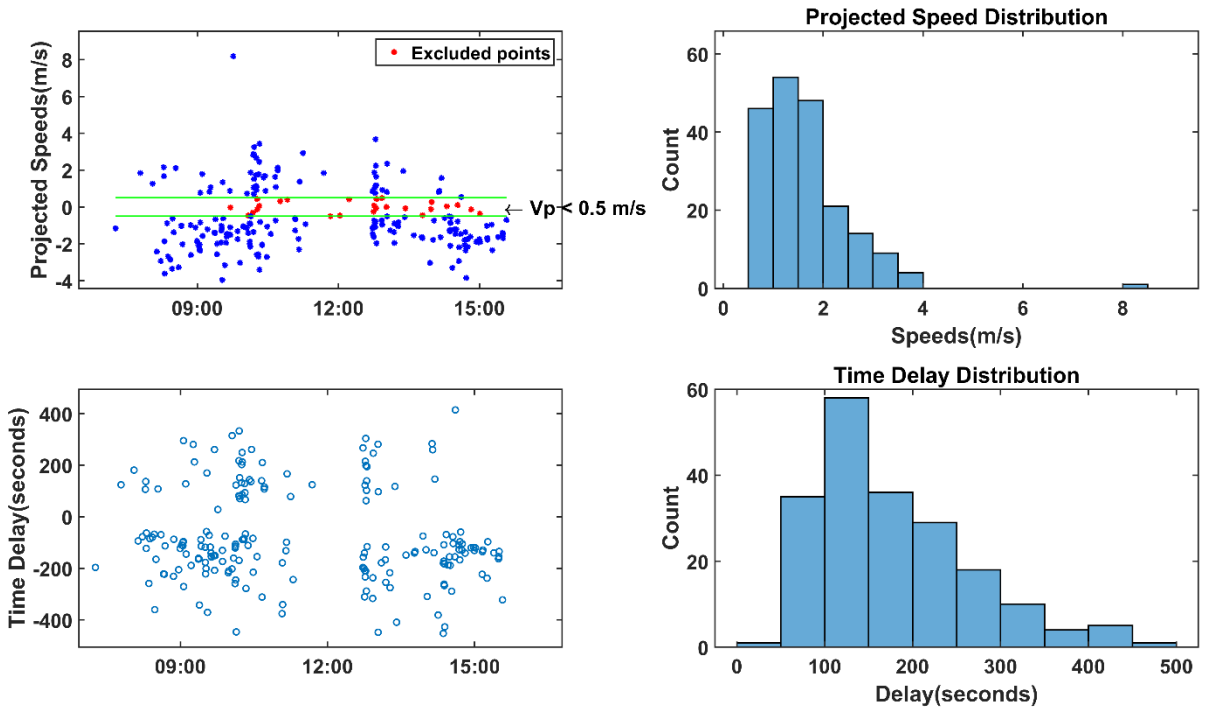

Figure 7: Projected Speeds after filtering with a minimum cutoff (top-left) and its magnitude distribution(top-right). Corresponding Time Delay from Cloud Motion Vectors(bottom-left) and its distribution(bottom-right)

Figure 7 shows the projected speeds for dataset 1, the values are bounded by a max speed of 4 m/s with one exemption, filtered values are marked in red on the top-right plot. The distances between the locations is known, so the time delay/lag can be calculated by dividing that separation distance by the projected speeds. From the bottom plots, the time delay varies between 0 to 500s in magnitude, the maximum delay is controlled by the minimum cut-off speed which is 0.5 m/s and the distance between locations which is 228 m. A distribution of the projection speeds shows most of the values in 0.5-2 m/s range and consequently most of the time lags are greater than 100s. These time delay values can now be used for comparison with those obtained from an analysis of the irradiance signals for both locations.

2.4 Time Lag from Signal Analysis

As mentioned in section 2.1, there is a necessity to pre-process the irradiance data before using it to derive time-lags. The irradiance signals from dataset 1 were reconstructed using the most prominent change-pts as described before. For the 9-hour window from 07:00 to 16:00, 504 points were selected, averaging to one change-point per minute. As shown in Figure 8, the modified signal is less noisy than the original signals. R-Squared values of the modified signal are very close to 1, indicating almost all the significant changes are captured.

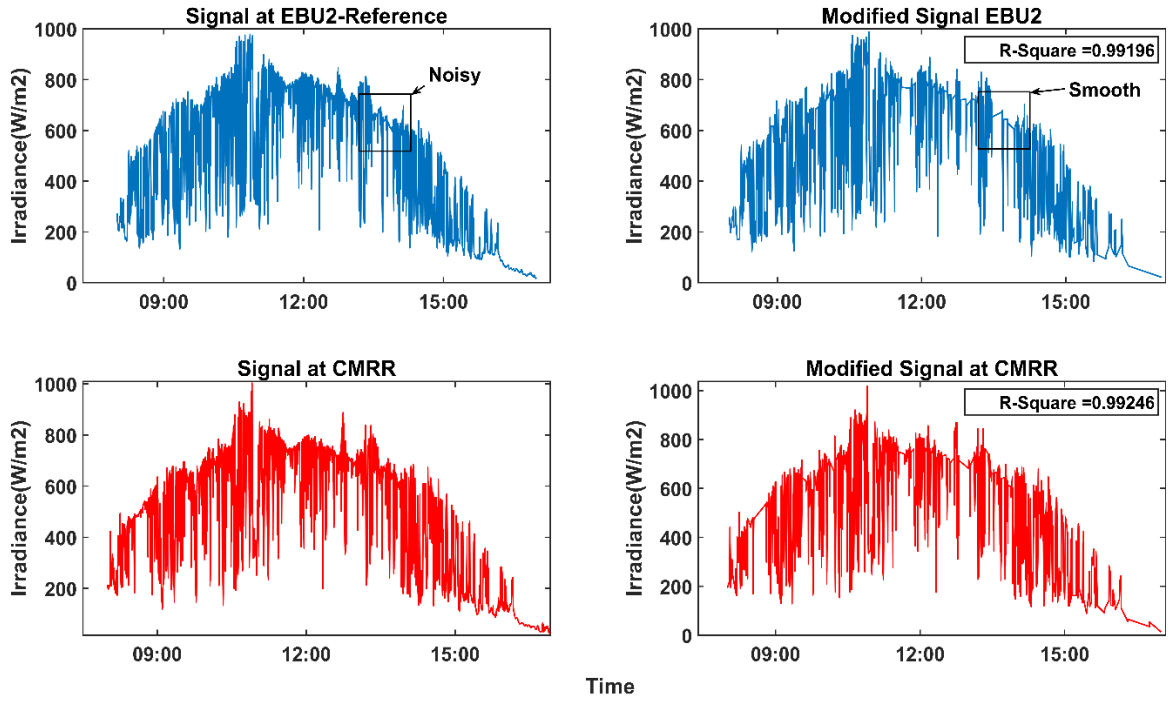

Figure 8 : Filtering Noise from Irradiance Data: Original Signals at Reference & Target (Left-Top, Left-Bottom), Modified Signals using changepoints(Right-Top, Right-Bottom).

The above signals were analyzed for similarities using the three methods described in Section 2.1. First method uses cross-correlation, in order to plot the variation of time lags the signals need to be correlated over fixed time windows throughout the entire day. In the first approach, Method 1a, the signal is divided into windows of 5 minutes and the time lags derived from correlation are plotted as shown in top-left plot of Figure 9. When there are no cloud phenomena the signals will be well aligned, and corresponding time lag should be zero or close to zero. Such windows of time lag less than 10s are removed from all the plots since they will not be useful when comparing with cloud speed derived lags in the following sections. In the second approach, Method 1b, correlation windows are placed around local minima of the signal, which were separated by a minimum of 5min to avoid overlap with neighboring windows. The lags in

the second case are have fewer points and most of them are located between 9:00-11:00 and 13:00 -15:00; the remaining periods didn't have many time lags greater than 10s.

In both cases there is a significant improvement in correlation coefficients from the initial lag to when the signal is shifted to get maximum correlation. It goes from mostly negative values to all positive values centered around 0.5, indicating better alignment after time-shifting the signal, Figure 9 shows the improvement in correlation coefficients. Although values are closer to 1 than before there is still some gap because of the initial dissimilarity in signals and that induced by the shifting around a previously aligned portion of the signal within the same window.

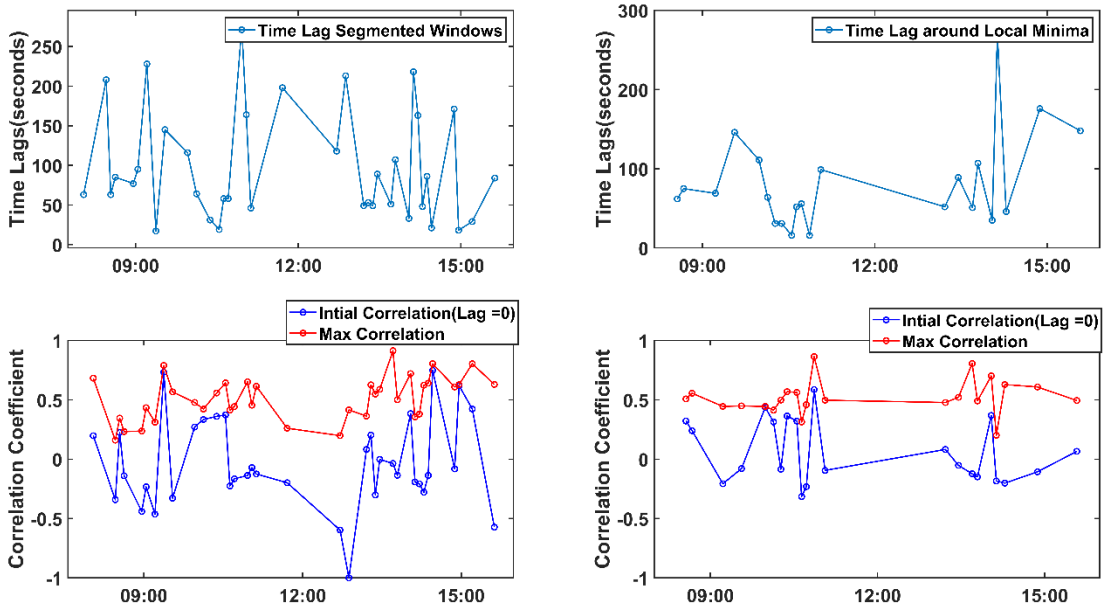

Figure 9: Time Lags from Cross-correlation (Method 1), Using Segmented Window Search (Top-Left) & Around Local Minima (Top-Right), Corresponding Improvement in Correlation coefficient (Bottom-Left & Bottom-Right)

The next method uses Euclidean distance (or RMSE value) between signals to compare similarities and determine the time-lag. Segmented windows of 5 minutes of the target signal (CMRR) are compared to time shifted values of reference signal (EBU2) to find the where the RMSE is minimum, the shift varies from -2.5 to + 2.5 minutes (Method 2a). In the second approach, Method 2b, the windows of 5 minutes are placed only around the local minima and which are separated by a minimum of 5 minutes (as explained previously in Method 1b). Figure 10 shows the derived time lags and the change in RMSE in both approaches. There are fewer points in Method 2b, since most of the windows had lags lower than the minimum cut-off of 10s. The change in RMSE is not prominent at all points. But the variation is centered around 4000 W2/m4 initially compared to the minimum RMSE which is centered around 2000 W2/m4 in both cases.

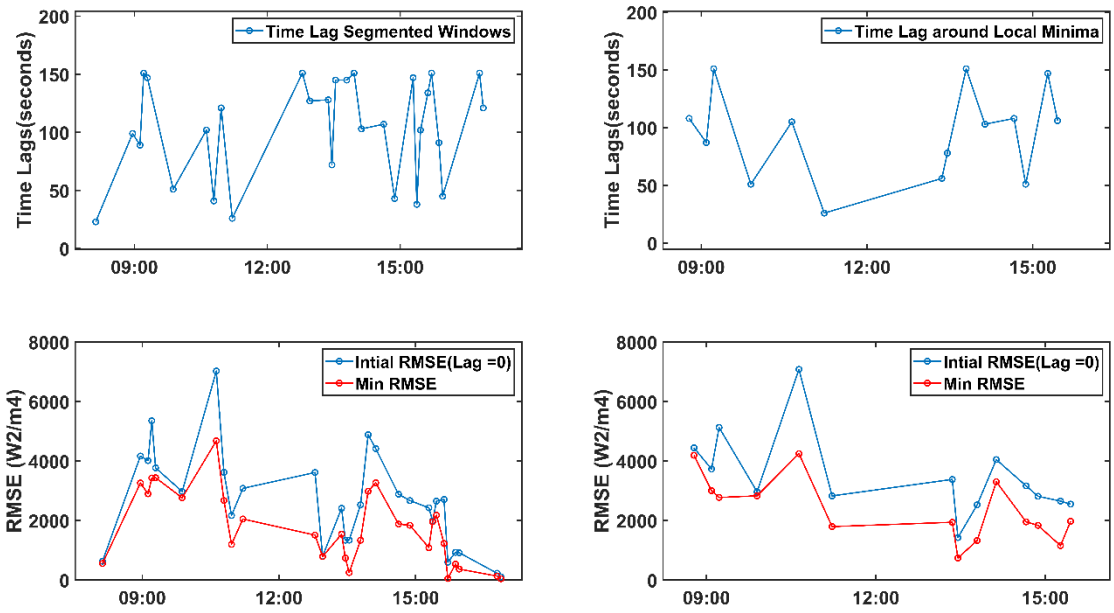

Figure 10: Time Lags from Minimizing Euclidean Distance (Method 2), Using Segmented Window Search (Top-Left) & Around Local Minima (Top-Right), Corresponding Improvement in RMSE (Bottom-Left & Bottom-Right)

The third method of comparing similarities between signals uses only the location of the local minima in both signals to find time lag. For each window of 5 minutes, the difference between the time stamp of the minimum point of different signals is the time lag for that window, Figure 11 shows the time lag variation and magnitude of irradiance at the local minima. Although, a similarity measure isn't calculated explicitly, the values of minimum irradiance for both signals are close in magnitude in most windows, implying good similarity between the signals at those points.

So far in this section, the time-lags from cloud motion vectors and from signal analysis using different similarity measures were derived. In the following section, both the values are compared to see if CMV's can be used predict the occurrence of dissimilarities in adjacent irradiance sensors.

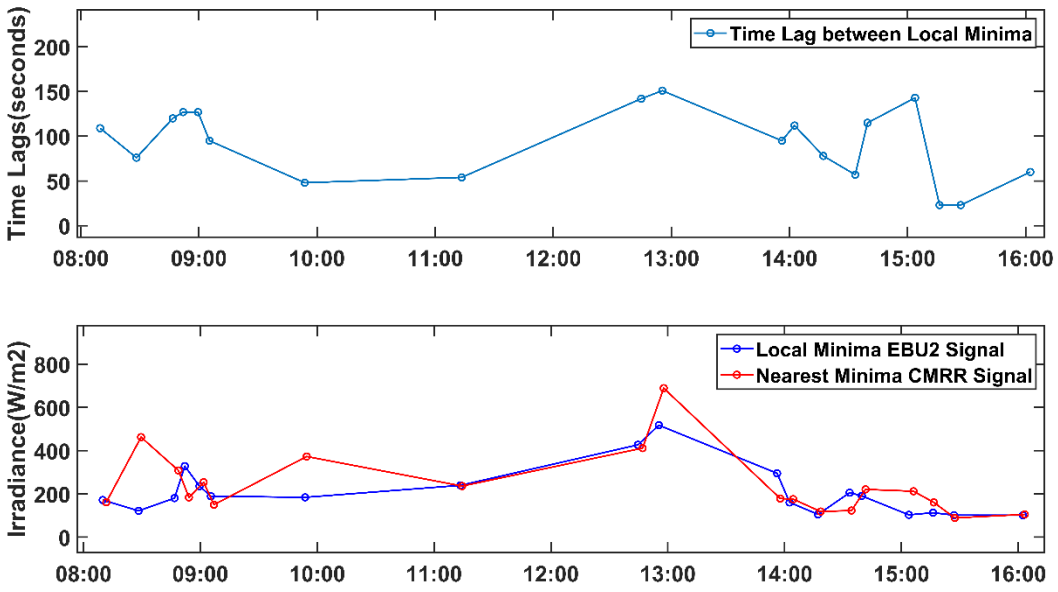

Figure 11: Time lags from Minima Matching (Method 3) (top), and the irradiance values at those local minima(bottom)

3. RESULTS

Input data from CMRR & EBU2 on 11th Oct 2017(Table 1), i.e. Irradiance Signals & Cloud Motion vectors have been independently used to track cloud movement between two locations and the outputs are time-lags that can be compared directly to understand their dependence. But time lags derived from CMV's are not found uniformly over the entire signal at the same times as the signal-derived values, so for each window from signal analysis the minimum time lag from CMV was selected in order to capture the maximum velocity recorded by the cloud sensor. Also, due to the circular setup of the cloud speed sensor there were some oscillations in sign that were ignored, only the magnitudes of time-lags are compared for both cases. Figure 12 shows the time-lag comparison for different methods, windows of 5 minutes were used for all the signal-analysis methods. The error metrics, RMSE, n-RMSE are displayed to the right of each plot; n-RMSE was calculated by dividing the RMSE by range of the CMV-derived time lag variation.

The performance of CMV- derived time lags in predicting signal derived time lags across different methods didn't vary much in terms of the n-RMSE value, it had an average of 0. 32 and standard deviation of 0.02. Using Euclidean Distance as the similarity measure for signal comparison had lower RMSE values, an average of 54s compared to 106s while using Cross-Correlation. Placing search windows around Local Minima reduced the RMSE & n-RMSE in case of Method 2 but increased error in Method 1. And Method 3, using only locations of local minima had an RMSE of 88s which is falls in between the performance of other two methods.

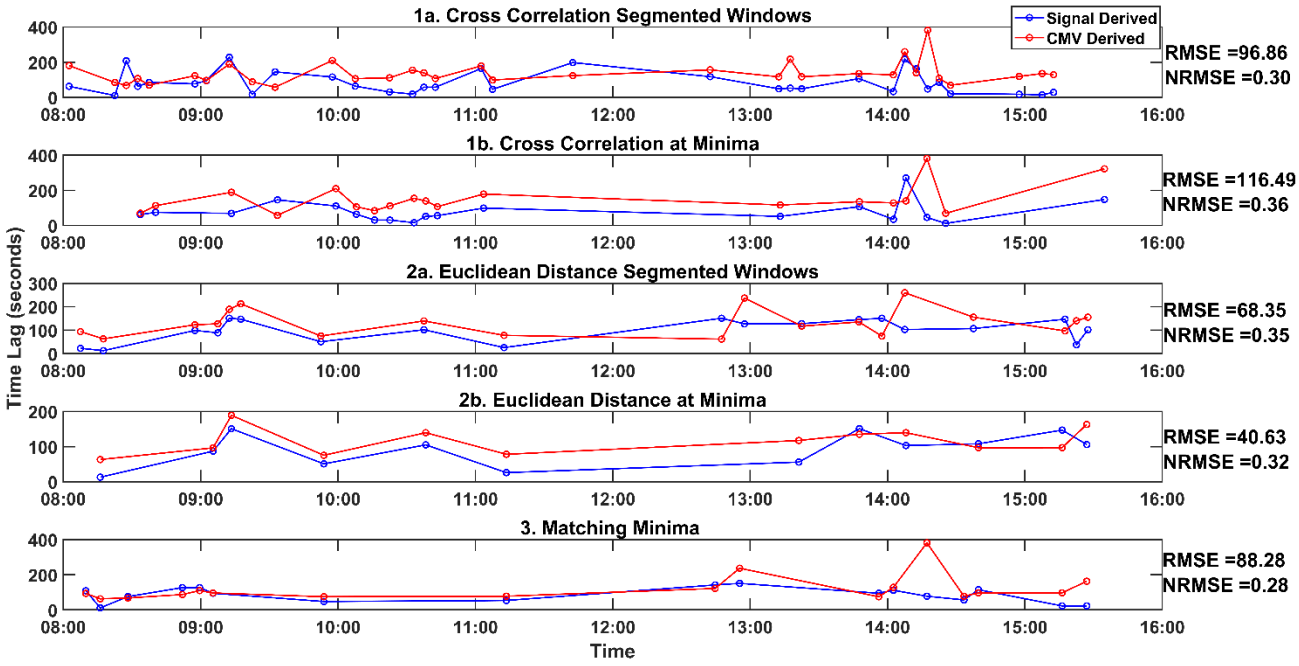

Figure 12: Time Lag Comparison Signal Analysis VS CMV Derived, using Cross-Correlation, Minimizing Euclidean Distance & Matching Local Minima and Error Metrics RMSE & n-RMSE are presented to the right of each plot.

The results were presented for one pair of locations (CMRR& EBU2) for one day (11th Oct 2017) and can be repeated for different locations with varied separation distances. From the data available, the above results were obtained for two more target locations TIOG and BMSB, which were 1.04 km and 681 m away from EBU2(reference) respectively but in different directions (Figure 4). As listed in Table 1, the data from BMSB is available on 8th, 10th & 11th Oct 2017 and the TIOG location on 8th Oct 2017. In addition to the CMRR data presented previously there are five days of data that were analyzed using the methodology discussed. In Figure 13 the n-RMSE values are plotted for all the different locations and days using the methods applied before. As distance between locations increases the time lags from CMV's will be proportionally higher,

and to locate the dissimilarities in the signal effectively the time window of analysis must be expanded accordingly. Time windows of 5-,10-,15-minutes were tested for each pair of locations and method and the best performing window was picked; 5 min for the CMRR location and 10 min for the other pairs.

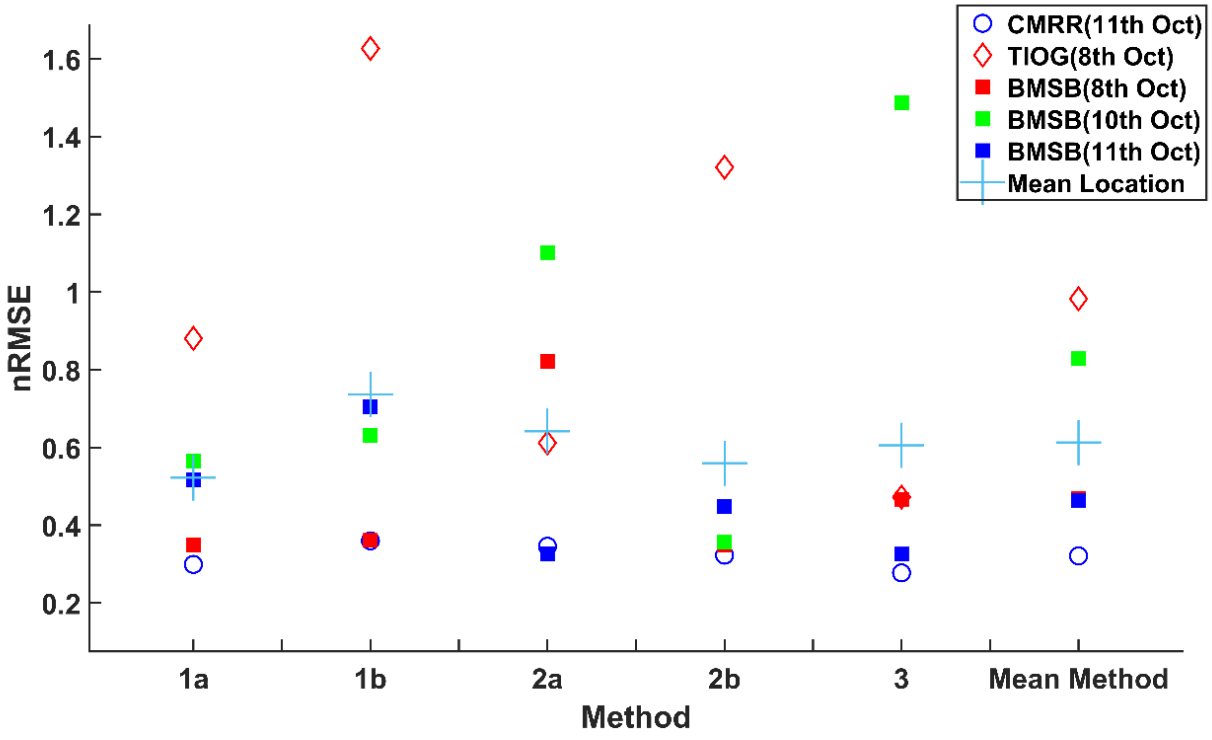

Figure 13: n-RMSE Variation with Signal Analysis Method for different Target Locations, CMRR, TIOG & BMSB. Date of availability is mentioned in parenthesis (Table 1)

The n-RMSE value changes drastically for different locations, the CMRR (11th Oct) data had the best performance with an average n-RMSE of 0.32. BMSB location had an average value of 0.59 over the three days (8th,10th,11th Oct), the rise in n-RMSE is expected since the distance from reference location (EBU2) is higher, 681m compared to CMRR, 228 m. For the TIOG Location, which is 1 km away, the n-RMSE values were the highest with an average of close to 1. Apart from the difference in separation distance, the direction vectors of the locations w.r.t to reference is also very different (Figure 4). A combination of these factors causes the wide-ranging differences in the results from different locations. In addition to the location dependence, the cloud conditions of different days also had a varied outcome as observed by the results from three days of data recorded at BMSB. Although the data from 8th & 10th Oct 2017 had a similar n-RMSE of 0.46, the values on 10th Oct were much higher with average of 0.82. Given the high n-RMSE values due to above factors, it is difficult to isolate the performance of different signal analysis methods from Figure 13. For the CMRR location which had the lowest n-RMSE values, the variation was not very significant as discussed previously.

4. CONCLUSION

When clouds move across irradiance sensors they cause drops in the signal that will be similar in nature if the distance between locations is small enough. In this study, the cloud speed data was used to find the estimated time it would take for such cloud-related irradiance drops to translate to nearby locations from a given reference location. Cloud speed derived time-lags provided a good estimate of the actual signal-derived time lags for a separation distance of 228m with an n-RMSE of 0.32 (average over different signal analysis methods). For the other two locations the n-RMSE values were much higher, growing proportionally with the separation distance. At 681 m, n-RMSE average to rose to 0.59 and at 1 km it reached close to 1. This is concurrent with previous studies that show that the correlation between the irradiance signals varies inversely with distance [8]. Signal analysis methods that use different similarity measures like Euclidean Distance, Cross-Correlation or the location of the Local Minima didn't have a significant variance when the separation distance was the shortest(228m), the errors were similar with a standard deviation of 0.02 in n-RMSE. For higher separation distances the errors were too high and varied across different methods to establish a relationship. But since limited data was used, further analysis spanning longer periods might provide better insights into their impact on the results.

After establishing a relation between the time-lags derived from CMV's and signal analysis, the next step would be to use CMV & irradiance data at a reference location to predict the occurrence of irradiance drops in a nearby irradiance sensor or a solar PV power signal. Power plant operators can schedule short term power ramps based on this data, but more information on the magnitude of these changes will be required. The irradiance signal at the reference location can provide more information on the variation but this can't easily be projected onto the target

since similarity between the signals is not consistent, it depends on the cloud conditions. Estimating dissimilarity between signals in real time would require more information about the cloud properties than just its speed and direction. For two given locations/irradiance sensors it might be possible to find the range of variation in similarity by analyzing the irradiance data over a span of time that covers a lot of different weather conditions.

Instead of using a single reference signal from one location, adding a network of sensors would provide additional avenues to forecast the irradiance drops at the target location. The time lags can be calculated using multiple sensor readings, providing the option to modify predictions for different cloud conditions. Also, the similarity measure between different signals can be tracked in real-time, and as in the case of time lags, a combination of the magnitude forecasts can be tested to find the best performing ones in different conditions. The performance of different reference signals in predicting the magnitude of irradiance drops of the target signal will depend on the topography of the sensor network in addition to the cloud conditions. If the network had layers with multiple sensors aligned in same direction, the forecasts can be validated while the cloud is on-route to the target location and recalibrated if required. Further analysis of irradiance and cloud motion data from dense networks of sensors recorded with high frequency over long time periods will provide deeper insights into their relationship and how it can be leveraged for solar power forecasting across different time windows.

REFERENCES

1. P. L. Joskow, "Comparing the Costs of Intermittent and Dispatchable Electricity Generating Technologies," *American Economic Review*, vol. 101, no. 3, pp. 238–241, 2011.

2. J. Kleissl, *Solar energy forecasting and resource assessment*. Amsterdam: Academic Press, 2013.

3. M. Diagne, M. David, P. Lauret, J. Boland, and N. Schmutz, "Review of solar irradiance forecasting methods and a proposition for small-scale insular grids," *Renewable and Sustainable Energy Reviews*, vol. 27, pp. 65–76, 2013.

4. C. W. Chow, B. Urquhart, M. Lave, A. Dominguez, J. Kleissl, J. Shields, and B. Washom, "Intra-hour forecasting with a total sky imager at the UC San Diego solar energy testbed," *Solar Energy*, vol. 85, no. 11, pp. 2881–2893, 2011.

5. G. Reikard, "Predicting solar radiation at high resolutions: A comparison of time series forecasts," *Solar Energy*, vol. 83, no. 3, pp. 342–349, 2009.

6. V. P. Lonij, A. E. Brooks, A. D. Cronin, M. Leuthold, and K. Koch, "Intra-hour forecasts of solar power production using measurements from a network of irradiance sensors," *Solar Energy*, vol. 97, pp. 58–66, 2013.

7. A. T. Lorenzo, W. F. Holmgren, and A. D. Cronin, "Irradiance forecasts based on an irradiance monitoring network, cloud motion, and spatial averaging," *Solar Energy*, vol. 122, pp. 1158–1169, 2015.

8. M. Lave, J. Kleissl, and E. Arias-Castro, "High-frequency irradiance fluctuations and geographic smoothing," *Solar Energy*, vol. 86, no. 8, pp. 2190–2199, 2012.

9. G. Wang, B. Kurtz, and J. Kleissl, "Cloud base height from sky imager and cloud speed sensor," *Solar Energy*, vol. 131, pp. 208–221, 2016.

10. S. Achleitner, A. Kamthe, T. Liu, and A. E. Cerpa, "SIPS: Solar Irradiance Prediction System," *IPSN-14 Proceedings of the 13th International Symposium on Information Processing in Sensor Networks*, 2014.